Size dependency of strain in arbitrary shaped anisotropic embedded quantum dots due to nonlocal dispersive effects

X. Zhang[1] and P. Sharma[1,2,*]
[1]*Department of Mechanical Engineering, University of Houston, Houston, Texas 77204, USA*
[2]*Department of Physics, University of Houston, Houston, Texas 77204, USA*
(Received 6 December 2004; revised manuscript received 1 September 2005; published 30 November 2005)

Both quantitative and qualitative knowledge of strain and strain distributions in quantum dots are essential for the determination and tailoring of their optoelectronic properties. Typically strain is estimated using classical elasticity and then coupled to a suitable band structure calculation approach. However, classical elasticity is intrinsically size independent. This is in contradiction to the physical fact that at the size scale of a few nanometers, the elastic relaxation is size dependent and a departure from classical mechanics is expected. First, in the isotropic case, based on the physical mechanisms of nonlocal interactions, we herein derive (closed-form) scaling formulas for strain in embedded lattice-mismatched spherical quantum dots. In addition to a size dependency, we find marked differences in both spatial distribution of strain as well as in quantitative estimates especially in cases of extremely small quantum dots. Fully recognizing that typical quantum dots are neither of idealized spherical shape nor isotropic, we finally extend our results to cubic anisotropy and arbitrary shape. In particular, an exceptionally simple expression is derived for the dilation in an arbitrary shaped quantum dot. For the more general case (incorporating anisotropy), closed-form results are derived in the Fourier space while numerical results are provided to illustrate the various physical insights. Apart from qualitative and quantitative differences in strain states due to nonlocal effects, an aesthetic by-product for the technologically important polyhedral shaped quantum dots is that strain singularities at corners and vertices (which plague the classical elasticity formulation) are absent. Choosing GaAs as an example material, our results indicate that errors as large as hundreds of meV may be incurred upon neglect of nonlocal effects in sub-10-nm quantum dots.

DOI: 10.1103/PhysRevB.72.195345 PACS number(s): 68.65.Hb, 61.46.+w, 85.35.−p, 62.25.+g

I. INTRODUCTION

Quantum dots (QDs) have been the focus of several experimental and theoretical researchers due to the promise of improved optoelectronic properties and are considered crucial building blocks for several nanoelectronic applications, e.g., next generation lighting,[1,2] lasers,[3,4] quantum computing, information storage and quantum cryptography,[5–7] biological labels,[8] sensors,[9] and many others.[10–15] QDs are typically embedded in another semiconductor material with differing lattice parameter. The ensuing elastic relaxation within the QD is well known to impact its optoelectronic properties. Several works, of varying sophistication (both analytical and numerical), have focused on the calculation of the strain state in buried quantum dots and the subsequent impact on optoelectronic properties.[16–25]

Strain has a direct effect on the band structure where conduction and valence bands are shifted and could be split apart, e.g., Ref. 26. Dilatation (i.e., hydrostatic strain) in QDs usually has the greatest effect although directional anisotropic effects in the typically cubic semiconductor crystals can be appreciable as well. In some material systems, the lattice distortion in and around buried QDs may also induce an electric field (e.g., GaN which is strongly piezoelectric). Generally speaking, researchers have used the well-established continuum elasticity theory (both numerically and analytically) to estimate mechanical strains. Those then are coupled to some suitable band structure calculation method (such as the tight-binding or $\mathbf{k}\cdot\mathbf{p}$ approach) to estimate the impact of strain on the optoelectronic properties. Classical continuum mechanics is, however, intrinsically size independent. This is in contradiction to the physical fact that at the size scale of a few nanometers, deformations and elastic state are size dependent and a qualitative departure from classical mechanics is expected. Various works (both experimental and theoretical) have addressed this issue in a wide range of contexts, e.g., nanoinclusions and nanowires,[27–31] thin films,[32–35] nanotubes,[36] composites,[28,37] and structural elements such as beams and plates.[38–40] In the particular context of nanoinclusions and quantum dots, this size dependency of mechanical strain at the nanoscale has been brought to light in recent publications by one of the authors.[21,28,41] The latter works presented the size-dependent elastic state of QDs based on the involvement of surface and interfacial energies at the nanoscale. For example, errors in strain calculation as high as 12% were reported in the determination of hydrostatic strain in a buried spherical QD (size range of 2 nm). To be more explicit, the dilatational strain in an isotropic spherical lattice-mismatched embedded quantum dot[42] that correctly incorporates the size effect due to interfacial energies can be written as[21,28]

$$\mathrm{Tr}(\boldsymbol{\varepsilon}) = 3\frac{3K\varepsilon^m - 2\tau_0/R}{4\mu + 3K + 2K^s/R}. \tag{1}$$

Here ε^m is the lattice mismatch and τ_0 is the surface or interfacial tension. K and μ are the bulk and shear modulus, respectively. K^s is the surface elastic modulus. Note that for large radius of QD ($R\to\infty$) or zero surface energy, the result reverts to the classical solution used by several authors.

Equation (1) was derived analytically by solving the boundary value problem of continuum elasticity *suitably modified* to incorporate interface energies. Further details on surface-energy-induced size effects and the subject of surface elasticity is suppressed for the sake of brevity. The reader is referred to several excellent works in the literature; see, for example, the more physically oriented reviews by Cammarata[34] and Ibach.[43] The work by Miller and Shenoy[40] presents a nice illustrative picture of surface elasticity in the context of simple structural elements such as beams and plates. A rigorous mathematical exposition can be found in Gurtin and Murdoch[44] and more recently in Gurtin *et al.*[45] The recent review article by Muller and Saul[46] is also very informative.

In the present work, we are interested in exploring another possible physical mechanism that may be responsible for inducing size effects in strains of QDs, namely, long-range nonlocal interactions. At small length scales (approaching a few nanometers comparable to the discrete structure of matter) the implicit long-wavelength assumption of classical elasticity breaks down. This breakdown is caused partially by the fluctuations in the interatomic interactions at the length scale of a few lattice spacings that are smoothed out at coarser scales (where classical elasticity is reasonably applicable). As one would expect, several phenomena at the level of a few lattice spacings are inadequately captured by classical elasticity and researchers often see enriched continuum theories like nonlocal elasticity as a replacement for atomistic simulations (or alternatively a bridge between atomistic and conventional continuum mechanics). For example, the ubiquitous singularities ahead of crack tips and dislocation cores (as predicted by classical mechanics) are indeed a breakdown of traditional elasticity at short wavelengths.[47] The obvious alternative method to compute strain is the use of atomistic simulations. An alternative (coarse-grained) field theoretic method is highly desirable (in the same vein as previous works,[16,18,19,21–25]) albeit that does also account for the scaling or size effects in strain likely to be prevalent at these small length scales (over and beyond surface or interfacial energy effects already addressed in Refs. 21, 28, and 41). The latter is the main objective of the present work. Postulating a form of strain gradient elasticity as a suitable model for small-scale elastic phenomena (which accounts for the long-range nonlocal interactions), we herein derive relations for the size-dependent strain in arbitrary shaped embedded lattice-mismatched quantum dots. Material anisotropy is also included.

The paper is organized as follows. In Sec. II, we present an idealized isotropic formulation and in particular discuss the rather illustrative example of a buried spherical quantum dot. This example is important as closed-form expressions can be derived and facilitate discussion of some of the features due to nonlocal effects. In Sec. III, nonlocal interactions are compared with interfacial energy effect and we also discuss, briefly, the combination of both. Arbitrary quantum dot shapes with arbitrary material anisotropy are considered in Sec. IV. We present numerical results for various shapes (but with isotropic material properties) in Sec. V while the discussion of anisotropic effects is the subject of Sec. VI. Given the scope of the present work and length of the paper, detailed coupled strain-band structure calculations are not presented though in Sec. VII, we provide the reader with a rough feel for the significance of our results for electronic band calculations. We finally conclude with a summary in Sec. VIII.

II. IDEALIZED ISOTROPIC FORMULATION WITH APPLICATION TO SPHERICAL QUANTUM DOTS

Assume a deeply buried arbitrary shaped quantum dot denoted by Ω. The interface of the quantum dot and the host matrix is S. Eventually in this section, to make analytical progress, we shall consider a spherical shaped quantum dot of radius R.

Consider for the moment a classical isotropic elastic material. The strain energy function is quadratic in strains:

$$W(\mathbf{x}) = \mu \varepsilon_{ij}\varepsilon_{ij} + \frac{1}{2}\lambda \varepsilon_{kk}^2. \tag{2}$$

Here, $\boldsymbol{\varepsilon}$ is the strain tensor related to $\mathbf{u}$ (displacement vector) as $\mathrm{sym}(\nabla \mathbf{u})$, μ and λ are the elastic Lamé constants and $[\cdot]_{,j}$ and ∂_j will be used interchangeably to indicate differentiation with respect to spatial variable x_j. Repeated indices indicate summation and Cartesian tensors are employed throughout. Note that the antisymmetric part of the deformation gradient, i.e., $\boldsymbol{\omega}$ (=asym $\nabla \mathbf{u}$) is absent from Eq. (2) since the quadratic term in $\boldsymbol{\omega}$ is not rotationally invariant—a necessary requirement for the energy function in Eq. (2). For small quantum dot sizes, additional gradient terms [absent in Eq. (2)] may also contribute and are considered to phenomenologically represent nonlocal interactions.[47,48] The latter is achieved by suitably adding higher-order terms containing gradients of strain and rotation.[49] The general form of the elastic energy involving first gradients of strain and rotation is

$$W(\mathbf{x}) = W(\partial_i u_j, \partial_l u_l, \partial_i \partial_l u_l, \partial_i \partial_l u_i). \tag{3}$$

In the isotropic case, the energy density, that is invariant to SO(3) and the T(3) groups, then takes the form[48]

$$W(\mathbf{x}) = \frac{\mu}{2}[(\partial_i u_j)^2 + \partial_j u_i \partial_i u_j] + \frac{\lambda}{2}(\partial_l u_l)^2 + \frac{2\mu+\lambda}{2} l'^2 \partial_i \partial_l u_l \partial_i \partial_j u_j + \frac{\mu l^2}{2}(\partial_l^2 u_i \partial_l^2 u_i - \partial_i \partial_l u_l \partial_i \partial_j u_j). \tag{4}$$

Two new coupling constants (in addition to the Lamé parameters) now appear namely, l' and l. Both have units of length. For band structure calculations in quantum dots, dilatation is the most important and in the isotropic case (as it turns out), the last term in Eq. (4) plays no role [see Eq. (29)] and hence we set $l=0$. Further, using a variational argument (by appealing to the Euler-Lagrange equations) the governing field equation can be derived as well as the response quantities (i.e., "stresses"). The balance laws that emerge are[48,50]

$$\sigma_{ij} = \sigma_{ij}^{\mathrm{cl}} + \delta_{ij}\partial_k \tau_k, \tag{5a}$$

$$\sigma_{ji,j} = 0. \tag{5b}$$

Here $\boldsymbol{\sigma}^{\mathrm{cl}}$ is the classical elastic stress which characterizes resistance of a deformable body to strain. Through incorporation of nonlocal effects via strain gradient terms, a new "stress" measure emerges, $\boldsymbol{\tau}$, that physically signifies a resistance to strain gradients.

The extended or modified elastic energy form in Eq. (4) yields the following constitutive relations:[48]

$$\sigma_{ij}^{\mathrm{cl}} = 2\mu u_{i,j} + \lambda \delta_{ij} u_{l,l}, \tag{6a}$$

$$\tau_i = (2\mu + \lambda) l'^2 \partial_i u_{l,l}. \tag{6b}$$

We now tackle the embedded quantum dot problem in this modified nonlocal elasticity formalism. There is a mismatch strain between the embedded quantum dot and the surrounding host material. The lattice mismatch strain tensor in the quantum dot (relative to zero reference strain in the host material) is given by the following relation:

$$\varepsilon_{ij}^{m} = \frac{2(a_{\mathrm{qd}} - a_{\mathrm{host}})}{(a_{\mathrm{qd}} + a_{\mathrm{host}})} \delta_{ij} = \varepsilon^{m} \delta_{ij}. \tag{7}$$

Here a is the lattice parameter. Noting that the mismatch strain is only nonzero within the quantum dot, we can write the modified elastic law as follows:

$$\begin{aligned} \sigma_{ij} = {} & 2\mu(u_{i,j} - \varepsilon_{ij}^{m} H) + \lambda \delta_{ij}(u_{l,l} - \varepsilon_{ll}^{m} H) \\ & + \delta_{ij}(2\mu + \lambda) l'^2 \nabla^2 (u_{l,l} - \varepsilon_{ll}^{m} H). \end{aligned} \tag{8}$$

Here H is the step function defined as

$$H(x) = \begin{cases} 1, & x \in \Omega, \\ 0, & x \notin \Omega. \end{cases}$$

Using Eqs. (5) and (6), we obtain a single equation in terms of the displacement vector:

$$\begin{aligned} & -\mu \partial^2 u_i - (\mu + \lambda) \partial_i \partial_l u_l + \underbrace{(2\mu + \lambda) l'^2 \nabla^2 \partial_i \partial_l u_l} \\ & \quad = 3K \delta_{ik} \partial_k [\varepsilon^{m} H(x)]. \end{aligned} \tag{9}$$

Here, $3K = 3\lambda + 2\mu$. The underlined portion of Eq. (9) indicates the extra terms absent in *size-independent* classical elasticity. Clearly, the derivatives of the mismatch strain $\varepsilon^{m} H(x)$ defined over the inclusion volume are δ functions across the QD-matrix interface: $\varepsilon^{m} \delta(S)$. The displacement vector can be obtained using the Green's function [of Eq. (9)] as

$$\begin{aligned} u_i(\mathbf{x}) &= 3K\varepsilon^{m} \delta_{jk} \int_S G_{ij}(\mathbf{x} - \mathbf{x}') dS_k(\mathbf{x}') \\ &= -3K\varepsilon^{m} \delta_{mn} \int_V G_{ij,k}(\mathbf{x} - \mathbf{x}') dV(\mathbf{x}'). \end{aligned} \tag{10}$$

Here the Gauss theorem has been used to convert the surface integral into a volume integral. Kleinert[48] derived the following expression for $\mathbf{G}$:

$$\begin{aligned} G_{ij}(\mathbf{x}, \mathbf{x}') = {} & \frac{1}{\mu r} \delta_{ij} - \frac{1}{2\mu} \partial_i \partial_j r \\ & + \frac{1}{2\mu + \lambda} \partial_i \partial_j \left[\frac{r}{2} + l'^2 \frac{1}{r} (1 - e^{-r/l'}) \right] \end{aligned} \tag{11}$$

where $r = |\mathbf{x} - \mathbf{x}'|$.

Mere substitution of Eq. (11) into Eq. (10) results in

$$\begin{aligned} u_i(\mathbf{x}) = {} & \frac{3K\varepsilon^{m}}{4\pi} \int dS_k(\mathbf{x}') \left\{ \frac{1}{\mu r} \delta_{ik} - \frac{\delta_{jk}}{2\mu} \partial_i \partial_j r \right. \\ & \left. + \frac{\delta_{jk}}{2\mu + \lambda} \partial_i \partial_j \left[\frac{r}{2} + l'^2 \frac{1}{r} (1 - e^{-r/l'}) \right] \right\} \\ = {} & 3K\varepsilon^{m} \left[-\frac{1}{\mu} \phi_{,k} \delta_{ik} + \frac{\delta_{jk}}{2\mu} \psi_{,ijk} - \frac{\delta_{jk}}{2\mu + \lambda} \left(\frac{\psi_{,ijk}}{2} + l'^2 \phi_{,ijk} \right. \right. \\ & \left. \left. - l'^2 M_{,ijk} \right) \right]. \end{aligned} \tag{12}$$

In the final expression on the right, the displacement field has been cast in terms of certain potentials defined below:

$$\begin{aligned} & \psi(\mathbf{x}) = \frac{1}{4\pi} \int_\Omega r \, dV(\mathbf{x}'), \quad \phi(\mathbf{x}) = \frac{1}{4\pi} \int_\Omega \frac{1}{r} dV(\mathbf{x}'), \\ & M(\mathbf{x}, l') = \frac{1}{4\pi} \int_\Omega \frac{e^{-r/l'}}{r} dV(\mathbf{x}'). \end{aligned} \tag{13}$$

$\psi(\mathbf{x})$ is the biharmonic potential, $\phi(\mathbf{x})$ is the Newtonian harmonic potential, while $M(\mathbf{x}, l')$ is the Yukawa potential. The first two potentials are well known in classical potential theory and the inclusion literature; see, e.g., Mura[51] and Kellogg.[52] The Yukawa potential is relatively less known and occurs in the study of non-Newtonian gravitation.[53] Recently, it has been employed in the study of inclusions in micropolar elasticity.[54,55]

Finally, the dilatation can be expressed as

$$\mathrm{Tr}(\boldsymbol{\varepsilon}) = -\frac{9K\varepsilon^{m}}{4\mu + 3K} \phi_{,ii} + \frac{9Kl'^2 \varepsilon^{m}}{4\mu + 3K} (M - \phi)_{,iikk}. \tag{14}$$

It is worth repeating that Eq. (14) is valid for *isotropic material properties but arbitrary shaped quantum dots*. To obtain explicit expression, we now specialize the derived expression in Eq. (14) to a spherical quantum dot.

For spherical shapes, the three potentials in Eq. (13) are[53–55]

$$\psi(r) = \begin{cases} -\frac{1}{60}(r^4 - 10R^2 r^2 - 15R^4), & r \in \Omega, \\ \frac{R^3}{15}\left(5r + \frac{R^2}{r}\right), & r \notin \Omega, \end{cases} \tag{15}$$

$$\phi(r) = \begin{cases} -\frac{1}{6}(r^2 - 3R^2), & r \in \Omega, \\ \frac{R^3}{3r}, & r \notin \Omega, \end{cases} \tag{16}$$

$$M(r,k) = \begin{cases} k^2 - k^2(k+R)e^{-R_0/k}\frac{\sinh(r/k)}{r}, & r \in \Omega, \\ k^2\left(R\cosh\frac{R}{k} - k\sinh\frac{R}{k}\right)\frac{e^{-r/k}}{r}, & r \notin \Omega. \end{cases} \tag{17}$$

After some algebra and manipulations, we finally obtain the following relation for the dilatation:

$$\mathrm{Tr}(\boldsymbol{\varepsilon}) = \begin{cases} \frac{9K\varepsilon^m}{3K+4\mu}\left(1 - (l'+R)e^{-R/l'}\frac{1}{l'}\frac{\sinh(r/l')}{r/l'}\right), & r \in \Omega, \\ \frac{9K\varepsilon^m}{3K+4\mu}\left(R\cosh\frac{R}{l'} - l'\sinh\frac{R}{l'}\right)\frac{1}{l'}\frac{e^{-r/l'}}{r/l'}, & r \notin \Omega. \end{cases} \tag{18}$$

Equation (18) is the major result of strain gradient elasticity for spherical QD. In Fig. 1 we plot the normalized dilations as a function of position and various quantum dot sizes. The dilation is normalized as $\mathrm{Tr}(\varepsilon_{ij})^* = \mathrm{Tr}(\varepsilon_{ij})(2\mu + \lambda)/3K\varepsilon^m$. Figure 1 is plotted parametrically in terms of the nonlocal coupling constant l'. The location $r/R=1$ indicates the boundary of the spherical quantum dot. The size effect of the nonlocal solution is manifest. We note that, unlike both the classical and interfacial energy-based solutions, the dilation incorporating nonlocal effects is inhomogeneous within the inclusion. Asymptotically, the nonlocal results converge to that of classical elasticity for large quantum dot size. Further, note that while the classical results predict the well-known zero dilatation outside the spherical quantum dot, in the case of nonlocal results we observe a small nonzero dilation. Conforming to physical intuition, artificial jumps in stresses are removed in nonlocal results and the strains vary smoothly across the interface, or in other words the "continuum" sharp interface of the quantum dot/matrix acquires a "diffuse boundary layer" to the order of the characteristic length scale parameter.

To emphasize the size dependency of our solution we also plot the dilatation as a function of size (for a fixed position, i.e., $r=0$) in Fig. 2. We observe that while for large quantum dot size, roughly $R > 7l'$, the nonlocal or strain gradient solution is indistinguishable from the classical one, the dilatation decreases significantly below this threshold and exhibits a marked departure from the classical solution.

In the preceding derivations and the remainder of the present work (in accord with several other researchers) we assume identical elastic constants for the quantum dot and the barrier material, which begets the question whether this kind of treatment is justified. This assumption of course is not a necessary requirement for our central concept or our approach. Clearly, for the ellipsoidal shape quantum dots

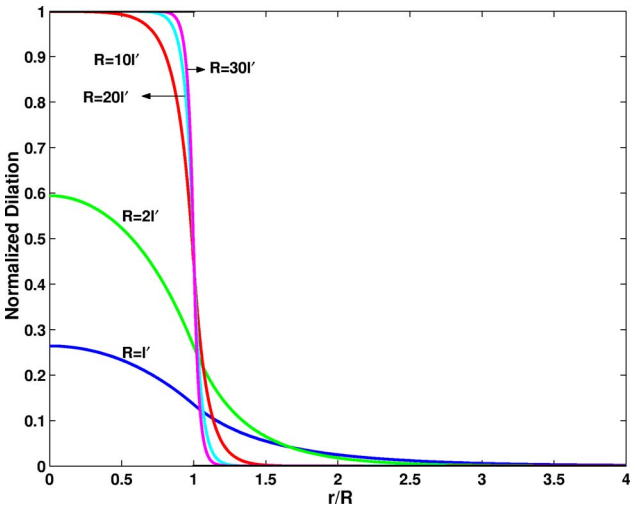

FIG. 1. (Color online) Strain dilatation (normalized by classical elasticity result) is plotted as a function of position and size.

embedded in an unbounded matrix, Eshelby's equivalent inclusion method[56] provides an easy recipe to account for modulus mismatch (of course only in the classical elastic context where the strain state is uniform for the ellipsoidal shape). More generally, as in the modified field theory used by us, this is not so easy. So are we justified in using the same elastic constants for both the materials? Faux *et al.*[57] argue that the Keyes scaling relationship[58,59] for III-IV semiconductors suggests that it is appropriate to choose the elastic constants of the barrier material for all materials in the system because all materials have the same lattice spacing before misfit strain relaxation takes place (see Ref. 57, p. 3758, Sec. D) and for materials in this group of the Periodic Table, the elastic constants are proportional to the nearest-neighbor lattice distance. As an illustration, the elastic constants for a strained InAs QD in a GaAs matrix will be closer to the GaAs values than those for unstrained InAs. In the present authors' opinion, this issue requires further investigation. In any case, if necessary, the modulus mismatch can be accounted for as a perturbation on our solution (see, for example, Andreev *et al.*[60] for a general procedure to do so).

Quite obviously the numerical values of the characteristic length scales determine the strength of the nonlocal or dispersive behavior of the crystal. Eringen[61] in his book provides an elementary discussion of this length scale. Of course this parameter is different for different materials. Generally the rough magnitude of this length scale is around the lattice parameter. Realistic values can only be obtained using detailed atomistic simulations. However, a crude one-dimensional Born-Karman-type chain model (presented by Eringen, Ref. 61, pp. 100–101) indicates this parameter to be exactly equal to the lattice parameter (a). Further, Eringen also indicates (p. 107) that matching nonlocal theories to experimental phonon dispersion curves yields $L=0.39a$ (unfortunately he does not specify which material other than indicating that it is of fcc structure). Altan and Aifantis[62] suggest a similar number. A better way to resolve this matter is through detailed lattice level models. DiVincenzo[63]precisely appears to have done so. In fact he

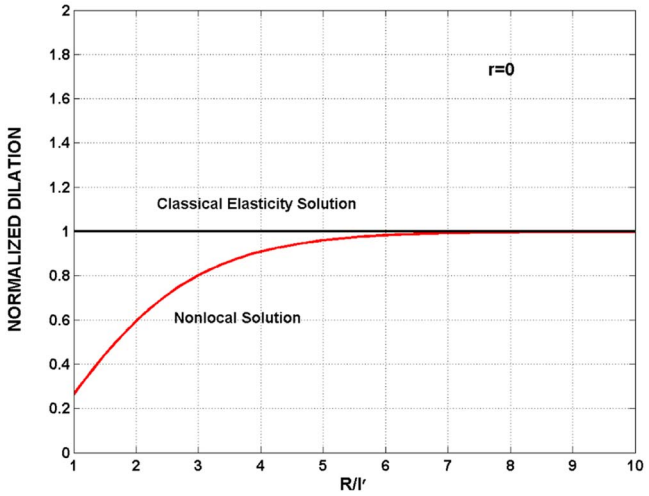

FIG. 2. (Color online) Dilatational strain as a function of size for fixed position ($r=0$). The results are normalized with respect to the classical elasticity solution.

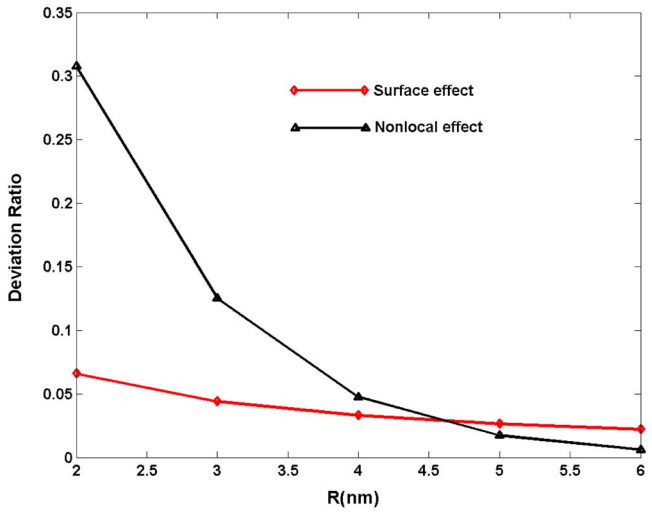

FIG. 3. (Color online) Deviation ratio is defined as $[\mathrm{Tr}(\varepsilon_{ij})_{\mathrm{classical}}-\mathrm{Tr}(\varepsilon_{ij})_{\mathrm{surface/nonlocal}}]/\mathrm{Tr}(\varepsilon_{ij})_{\mathrm{classical}}$. The mismatch strain is 0.067 nm (typical for the InAs/GaAs system). Internal length scale is 0.82 nm. Interfacial tension is 1 J/m^2. Material properties are based on isotropic data in Table I.

addresses dispersivity (nonlocality) in the semiconductor material GaAs (an important quantum dot material). To understand this issue further, a discussion of a key concept is in order. If one uses classical elasticity, one obtains as dispersion relation[64]

$$\rho\omega^2 = ck^2. \tag{19}$$

Here ω is the frequency, k is the magnitude of the wave vector, while ρ is the material density. Obviously c is related to the classical elastic modulus. Thus there is a linear relation between wave vector and frequency in classical elasticity, i.e., there is no dispersion and hence no nonlocal effects. When dispersion or nonlocal effects are incorporated, this relation gets modified:

$$\rho\omega^2 = ck^2 + fk^4. \tag{20}$$

The material parameter f is the higher-order elastic parameter characterizing the strength of dispersion effects. Now the square root of the ratio f/c provides a measure of this length scale. Again, we refer the reader to Eringen's book[61] for a discussion on how one can evaluate this length scale through phonon dispersion curves (pp. 98–99). Using the work by DiVincenzo[63] (p. 5462), we can evaluate this length scale for GaAs to obtain ~0.82 nm.

III. COMPARISON WITH INTERFACIAL ENERGY EFFECT AND COMBINATION OF BOTH EFFECTS

We now proceed to draw a comparison between surface energy effects [embodied in Eq. (1)] and nonlocal results. Unfortunately, while the nonlocal results can be adequately normalized (i.e., independent of mismatch strain), the surface and interfacial results cannot and are highly material dependent (both on the actual values of interfacial energy parameters as well elastic moduli). We provide some general estimates here. As mentioned in the previous section, the nonlocal coupling constant l' roughly corresponds to the lattice parameter of the quantum dot which is around ~0.4 nm for most materials. At least in one instance (for the case of GaAs), based on the work of DiVincenzo,[63] we can estimate it to be ~0.82 nm. The interfacial tension (for coherent systems) is roughly to the order of ~1 J/m^2.[56] Since (unlike both the classical- and surface-energy-based results) the nonlocal solution is nonuniform, we compare results at the quantum dot center ($r=0$). A comparison is depicted in Fig. 3. Due to the exponential decay in the nonlocal solution (with respect to size), the nonlocal effects decay far more rapidly than the interfacial effects but are likely to dominate for very small sizes only. This is highly material dependent and depends crucially on the relative magnitude of the interfacial tension and the nonlocal coupling constant. Most results will be presented for GaAs (which has a rather high l') and thus nonlocal effects are seen to be appreciable.

At least for the simple spherical shape, the combination of nonlocal effects and interfacial energy effect is relatively simple (mainly due to an elegant result of Eshelby[56]). Interfacial tension is a residual effect and is (like the lattice mismatch strain) a nonelastic contribution. For example, consider for the moment that nonlocal effects are absent. For the spherical shape then, the actual elastic state of the quantum dot can be obtained by assuming that the lattice mismatch strain) a non-elastic contribution. For example, consider for the moment that nonlocal effects are absent. For the spherical shape then, the actual elastic state of the quantum dot can be obtained by assuming that the lattice mismatch strain instead of being the nominal ε^m is actually $\varepsilon^m - 2\tau_0/3KR$. Using this, one can trivially recover the expression in Eq. (1). Now to incorporate nonlocal interactions, one simply substitutes the "effective" lattice mismatch strain $\varepsilon^m - 2\tau_0/3KR$ in Eqs. (7)–(14) to obtain the following result for the combined nonlocal-interfacial effect:

$$\mathrm{Tr}(\boldsymbol{\varepsilon}) = \begin{cases} \dfrac{9K(\varepsilon^m - 2\tau_0/3KR)}{3K+4\mu}\left(1-(l'+R)e^{-R/l'}\dfrac{1}{l'}\dfrac{\sinh(r/l')}{r/l'}\right), & r \in \Omega, \\ \dfrac{9K(\varepsilon^m - 2\tau_0/3KR)}{3K+4\mu}\left(R\cosh\dfrac{R}{l'} - l'\sinh\dfrac{R}{l'}\right)\dfrac{1}{l'}\dfrac{e^{-r/l'}}{r/l'}, & r \notin \Omega. \end{cases} \tag{21}$$

Due to the linearity of our system of equations, one is hardly surprised by the simplicity of this result. The combined effect is plotted in Fig. 4 and compared with the case when nonlocal or interfacial effects alone are considered for various values of the mismatch strain.

The normalized trace of the strain at the center of the QD is plotted in Fig. 5 with mismatch strain of 0.067 (which corresponds to the InAs/GaAs system). Since for this material system, nonlocal interaction effects dominate, the surface energy terms do not contribute significantly. This conclusion may of course alter for different material property combinations.

IV. ARBITRARY SHAPE AND ANISOTROPY: GENERAL FORMULATION

In the previous section we considered the idealized spherical shape. The reader is referred to Refs. 14 and 65–69 which report evidence of a wide variety of shapes, including pyramidal, truncated pyramidal, lens shaped, hemispherical, multifaceted domes, etc., for the widely studied $In_xGa_{1-x}As/InAs$ quantum dot system.

For some cases, the assumption of elastic isotropy may be justified or alternatively the uncertainty in other material and configurational parameters (e.g., lattice parameters, dimensions, etc.) may far exceed the error due to neglect of the anisotropic effects. In general most semiconductor compounds are cubically anisotropic. Against the isotropic value of 1, the anisotropy coefficient [defined as $(C_{11}-C_{12})/2C_{44}$] for most III-IV semiconductors is around 0.5.

To ensure a broader applicability of our work, we extend our nonlocal analysis of embedded quantum dots to incorporate arbitrary shape and anisotropy. In particular, we shall emphasize cubic anisotropy. We first, however, discuss arbitrary shape in the isotropic limit.

As derived in previous section, in the strain gradient or nonlocal formalism, the strain tensor can be written as

$$\varepsilon_{ik} = -\frac{1}{2}\int_\Omega [G_{ij,lk}(r) + G_{kj,li}(r)]P^m_{jl}dV(\mathbf{x}'). \tag{22}$$

Here P^m_{jk} is related to the mismatch strain through the elastic moduli: $P^m_{ij}=C_{ijkl}\varepsilon^m_{kl}$. The effect of shape emerges in form of the integration domain of the integral in Eq. (20). To separate the shape effect in Eq. (22), we follow Andreev *et al.*[60] who performed a similar analysis in the classical elasticity context.

The Fourier transform of Eq. (22) yields

$$\hat{\varepsilon}_{ik} = \frac{1}{2}(q_l q_k \hat{G}_{ij} + q_l q_i \hat{G}_{kj})P^m_{jl}\hat{\chi}(\mathbf{q}). \tag{23}$$

Here $\mathbf{q}$ is the wave vector and the following Fourier transform pair are employed in the present work:

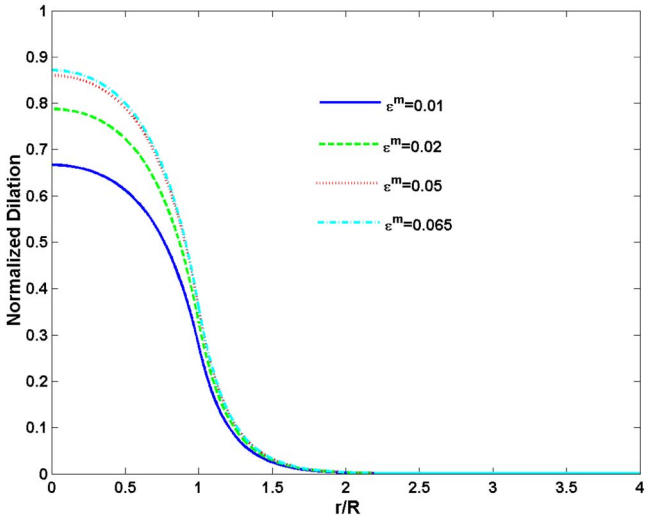

FIG. 4. (Color online) Strain dilation of a spherical QD based on combination of nonlocal and surface effects. Normalized strain is defined as $\mathrm{Tr}(\varepsilon_{ij})(3K+4\mu)/9K\varepsilon^m$. The materials properties are based on the isotropic case in Table I. The QD is chosen with radius as $R=4l'$ and the internal length scale is chosen as $l'=0.82$ nm.

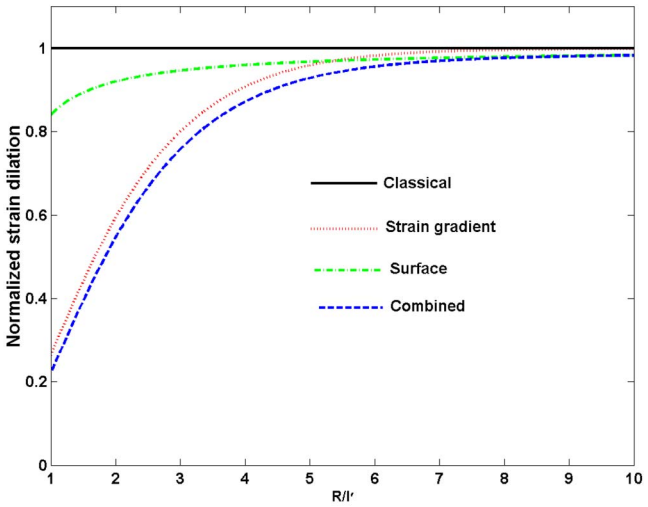

FIG. 5. (Color online) Strain dilation at center of QD with mismatch strain equal to 0.067. Material properties are based on Table I. Internal length scale is $l'=0.82$ nm.

$$u_i(\mathbf{x}) = \int \frac{d^3\mathbf{q}}{(2\pi)^3} e^{i\mathbf{q}\cdot\mathbf{x}} \hat{u}_i(\mathbf{q}),$$

$$\hat{u}_i(\mathbf{q}) = \int d^3\mathbf{x}\, e^{-i\mathbf{q}\cdot\mathbf{x}} u_i(\mathbf{x}). \tag{24}$$

$\hat{\chi}(\mathbf{q})$ is the so-called characteristic shape function. It is exactly the Fourier transformation of the Heaviside function for different shapes:

$$\hat{\chi}(\mathbf{q}) = \int_\Omega e^{-i\mathbf{q}\cdot\mathbf{x}} dV(\mathbf{x}). \tag{25}$$

For many common QD shapes, Andreev *et al.*[60] have provided analytical expressions for $\hat{\chi}(\mathbf{q})$. Essentially, the "shape" information is wholly contained in the characteristic shape factor $\hat{\chi}(\mathbf{q})$ while the remaining expression [in Eq. (23)] contains solely non-shape-dependent physics. For the orthogonal polyhedral shape for which Andreev *et al.*[60] did not provide an expression, we have derived the following result:

$$\hat{\chi}(q,a,b,c) = \frac{[iabe^{-icq_3}q_1q_2(aq_1-bq_2) + iace^{-ibq_2}q_1q_3(cq_3-aq_1) + ibce^{-iaq_1}q_2q_3(bq_2-cq_3) + (bq_2-cq_3)(aq_1-bq_2)(cq_3-aq_1)]}{q_1q_2q_3(bq_2-cq_3)(aq_1-bq_2)(cq_3-aq_1)} \tag{26}$$

where a, b, c are intercepts of the orthogonal polyhedral on the x, y, z coordinates.

Once again, Kleinert's Green's function[48] in Fourier space is

$$\hat{G}_{ij} = \frac{1}{\mu q^2(1+l^2\mathbf{q}^2)}\delta_{ij} + \frac{q_iq_j}{q^4}\left(-\frac{1}{\mu(1+l^2\mathbf{q}^2)} + \frac{1}{(2\mu+\lambda)(1+l'^2\mathbf{q}^2)}\right). \tag{27}$$

Substituting Eq. (27) in Eq. (23) leads to an analytical expression for the Fourier strain field of a QD for an arbitrary shape:

$$\hat{\varepsilon}_{ik}(\mathbf{q}) = P^m_{jl}\hat{\chi}(\mathbf{q})\left[\frac{\delta_{ij}q_lq_k + \delta_{kj}q_lq_i}{2\mu\mathbf{q}^2(1+l^2\mathbf{q}^2)} + \frac{q_iq_jq_kq_l}{\mathbf{q}^4}\left(-\frac{1}{\mu(1+l^2\mathbf{q}^2)} + \frac{1}{(2\mu+\lambda)(1+l'^2\mathbf{q}^2)}\right)\right]. \tag{28}$$

Noting that the lattice mismatch strain tensor is hydrostatic, i.e., $P^m_{ij} = P^m\delta_{ij} = C_{ijkl}\varepsilon^m\delta_{kl} = 3K\varepsilon^m$, the strain tensor adopts a particularly simple form:

$$\hat{\varepsilon}_{ik}(\mathbf{q}) = P^m\hat{\chi}(\mathbf{q})\frac{q_iq_k}{\mathbf{q}^2}\left(\frac{1}{(2\mu+\lambda)(1+l'^2\mathbf{q}^2)}\right). \tag{29}$$

As l' approaches 0, Eq. (29) approaches the classical solution obtained by Andreev *et al.*[60] If one is only interested in strain dilation, we obtain

$$\hat{\varepsilon}_{kk}(\mathbf{q}) = P^m\hat{\chi}(\mathbf{q})\left(\frac{1}{(2\mu+\lambda)(1+l'^2\mathbf{q}^2)}\right). \tag{30}$$

Numerical results for various shapes are presented in the next section. The reverse Fourier transformation of Eq. (30) immediately yields the nonlocal solution of the strain dilation of the QD as

$$\mathrm{Tr}(\varepsilon_{ij}) = \frac{P^m}{(2\mu+\lambda)l'^2}M(\mathbf{x},l'). \tag{31}$$

Thus the dilatation of *any shape* is reduced to the evaluation of the Yukawa potential. This result is rather interesting. We note here that the dilation in the classical elasticity context is *shape independent* and thus rather simple to evaluate. The nonlocal results (while also simple by all means) show a dependence on shape.

We now focus on anisotropic effects. Common QD materials are cubically anisotropic and are characterized by three independent elastic moduli C_{1111}, C_{1212}, and C_{1122}, instead of two independent moduli for isotropic materials. Insofar as strain gradient constants are concerned, six are required instead of two that emerge in the isotropic case.

Using DiVincenzo[63] and discarding the dynamic parts, the elastically anisotropic Lagrangian that incorporates gradient effects is

$$-L = \frac{1}{2}C_{ijkl}u_{i,j}u_{k,l} + D_{ijklm}u_{i,j}u_{k,lm} + F^1_{ijklmn}u_{i,j}u_{k,lmn} + F^2_{ijklmn}u_{i,jk}u_{l,mn} + A_{ijklmn}u_{i,j}u_{k,l}u_{m,n} + \cdots \tag{32}$$

where C_{ijkl} is the classical stiffness matrix. D_{ijklm}, F^1_{ijklmn}, F^2_{ijklmn}. and A_{ijklmn} are strain gradient elastic tensors. As before, using the variational formalism, we obtain the following Navier-like equations:

$$C_{ijkl}u_{k,jl} + d_{ijklm}u_{k,jlm} + f_{ijklmn}u_{k,jlmn} + b_i = 0 \tag{33}$$

where d_{ijklm} and f_{ijklmn} are related to higher-order anisotropic strain gradient components through

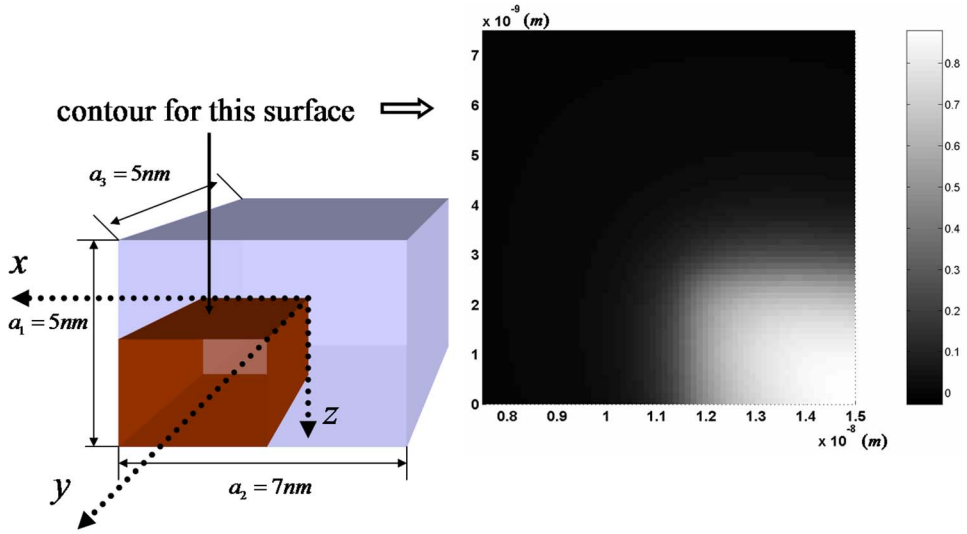

FIG. 6. (Color online) Strain gradient results for dilation strain of cuboidal quantum dot. Dilation strain is normalized as $\mathrm{Tr}(\varepsilon_{ij})(2\mu+\lambda)/P^m$ Light area represents high dilation. Internal length scale is $l'=0.82$ nm.

$$d_{ijklm} = D_{ijklm}, \tag{34}$$

$$f_{ijklmn} = F^1_{ijklmn} - F^2_{ijklmn}.$$

b_i in Eq. (33) is the body force which can be related to the mismatch strain. In Fourier space, Eq. (33) is rewritten as

$$C_{ijkl}q_jq_l\hat{u}_k + id_{ijklm}q_jq_lq_m\hat{u}_k - f_{ijklmn}q_jq_lq_mq_n\hat{u}_k = \hat{b}_i. \tag{35}$$

The equivalent body force due to the lattice mismatch strain is (see Sec. II for the corresponding one in the isotropic case):

$$\hat{b}_i = -iq_lP^m_{il}\hat{\chi}(\mathbf{q}). \tag{36}$$

Finally the displacement field for the anisotropic material is

$$D_{ik}\hat{u}_k = -iq_lP^m_{il}\hat{\chi}(\mathbf{q}) \tag{37}$$

where D_{ij} is

$$D_{ik} = C_{ijkl}q_jq_l + id_{ijklm}q_jq_lq_m - f_{ijklmn}q_jq_lq_mq_n. \tag{38}$$

The final strain tensor in Fourier space is

$$\hat{\varepsilon}_{ij} = iq_j\hat{u}_i + iq_i\hat{u}_j. \tag{39}$$

This completes our formulation and numerical results for anisotropic effects are presented in Sec. VI.

V. ARBITRARY SHAPE: NUMERICAL RESULTS

In order to separate the shape effects from anisotropy, first we present results for the isotropic case for various shapes. The derived equations are numerically solved using spectral methods (see, for example, Ref. 70). Equation (31) can be rewritten explicitly as

$$\mathrm{Tr}(\varepsilon_{ij}) = \frac{P^m}{4\pi(2\mu+\lambda)l'^2}\int_\Omega \frac{e^{-r/l'}}{r}dV(\mathbf{x}'). \tag{40}$$

For numerical calculations, a periodic distribution (n_xd, n_yd, n_zd) of quantum dots is used. Each unit cell (d,d,d) is uniformly meshed into a $128\times128\times128$ grid. d is chosen large enough (25 nm) to render interaction effects between the quantum dots negligible.

A. Cuboidal quantum dot

The sample quantum dot is chosen with edge line lengths $a_1=5$ nm, $a_2=7$ nm, and $a_3=5$ nm. The dilation contour plot is given for 1/4 of the cuboidal QD in Fig. 6 which indicates that the nonlocal dilation solution decays smoothly across the boundary of the QD. In contrast, as is well known the classical solution for dilation is a constant inside the QD, while zero outside.

The spatial distribution of the strain dilation in the cuboidal quantum dot is shown in Fig. 7. The contrast between strain gradient elasticity and classical elasticity

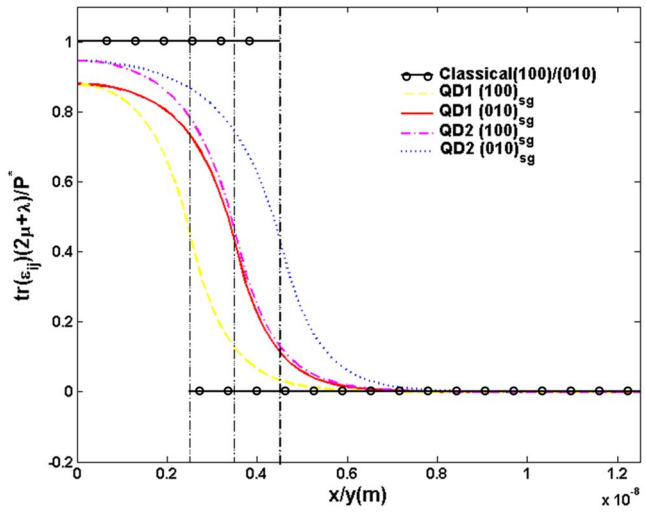

FIG. 7. (Color online) Normalized strain dilation is plotted for two directions on the crossing plane $z=0$. The subscript "sg" indicates strain gradient while "cl" indicates classical. Vertical dotted lines mark the boundary of QD at two directions (x and y). QD1's size is $a_1=5$ nm, $a_2=7$ nm, and $a_3=5$ nm. QD2's size is $a_1=7$ nm, $a_2=9$ nm, and $a_3=7$ nm.

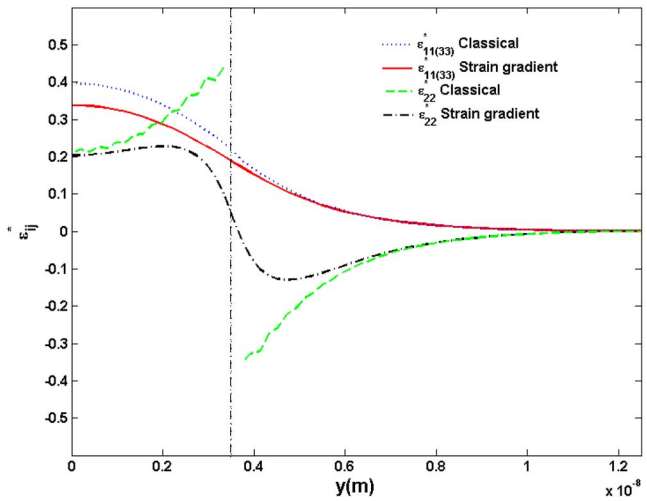

FIG. 8. (Color online) Strain components ε_{11} and ε_{33} of cuboidal QD with $a_1=5$ nm, $a_2=7$ nm, and $a_3=5$ nm. Vertical dotted line is the boundary of the QD. The plot is along (010).

solutions[60,71,72] is manifest. Unlike the classical result (where dilation is uniform for all shapes), the strain gradient results show sensitivity with respect to direction even for this isotropic case (and indeed we have chosen a sample cuboidal QD, which is not symmetric, to precisely illustrate this).

The individual strain components are exhibited in Fig. 8. Classical results are also provided for comparison. Since in our example two edges of the QD are of the same length, ε_{11} is identical to ε_{33}. The difference between the classical result and strain gradient result for ε_{11} and ε_{33} is not too large, but appreciable for ε_{22}, especially near the boundary of the QD. As in earlier examples, the discontinuity at the boundary of QD is removed by strain gradient elasticity. In Fig. 8, some ripples near the point of discontinuity can be observed. This is the so-called Gibbs phenomenon common in use of the spectral method and caused by numerical truncation in the Fourier domain. This effect only occurs when a function is not smooth and continuous.[73] Hence, it does not appear in the strain gradient results.

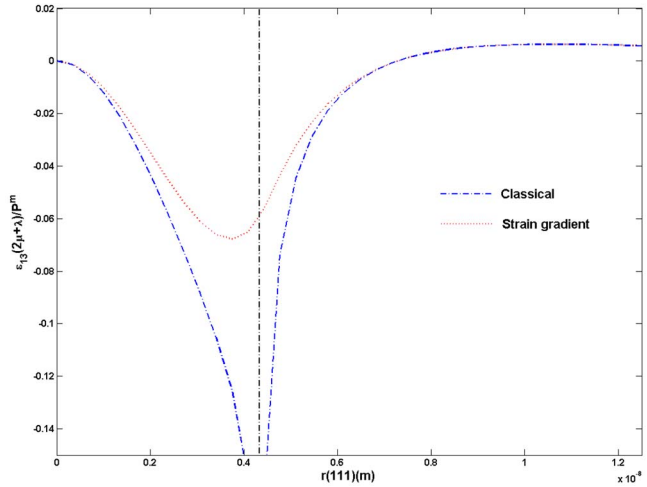

FIG. 9. (Color online) Strain components ε_{13} along (111) direction of cuboidal QD with edge length equal to 5 nm.

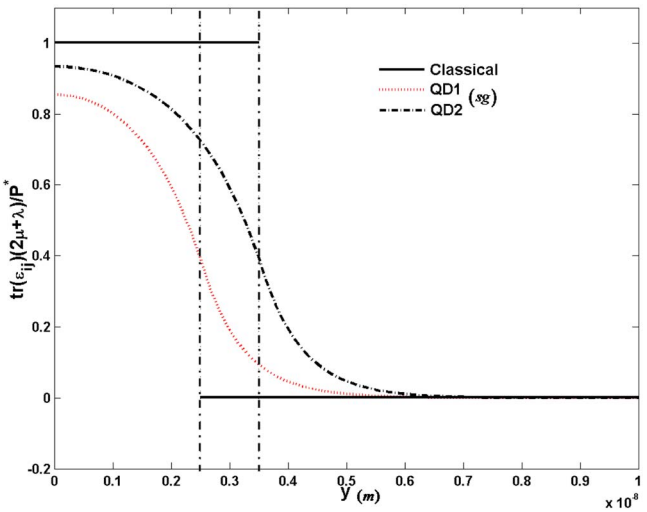

FIG. 10. (Color online) Dilation strain for finite cylindrical QD1, with diameter $D=5$ nm and height $h=8$ nm, and QD2, with $D=7$ nm and $h=10$ nm.

Finally we point out that our nonlocal formulation is capable of removing the "pesky" singularities at the corners and edges of the realistic shaped QDs (Fig. 9). It is well known that sharp edged and cornered inclusions or quantum dots exhibit weak logarithmic singularities at these junctions. As illustration we show a specific example for a cubic QD with edges $a_1=a_2=a_3=5$ nm. We plot the strain ε_{13} along the (111) direction, which passes one corner of the cube. As expected from classical elasticity result,[18] ε_{13} diverges at the corner while our nonlocal solution behaves in a more physically reasonable manner. Generally researchers who employ classical elasticity to compute the strain state in polyhedral quantum dots typically truncate their computation around a small region surrounding this divergence. Our results render such a procedure redundant.

B. Finite-length cylindrical quantum dot

The strain gradient solution for an infinite-length cylindrical quantum dot is much simpler, since the integral in Eq.

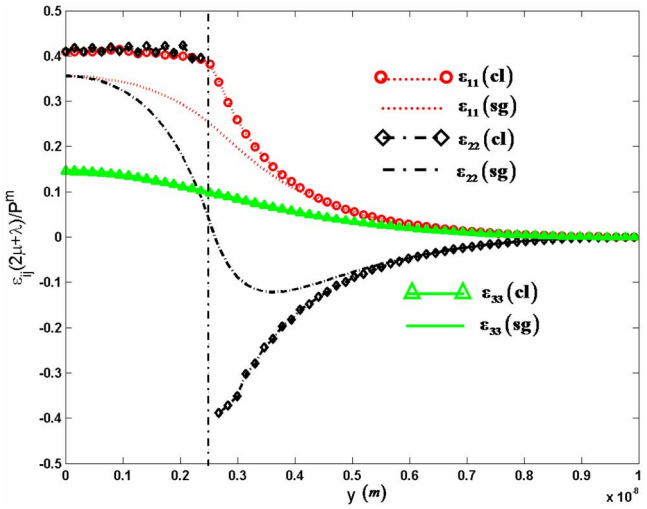

FIG. 11. (Color online) Strain components for finite cylinder QD with $D=5$ nm and $h=8$ nm. [ε_{33} (cl) overlaps with ε_{33} (sg).]

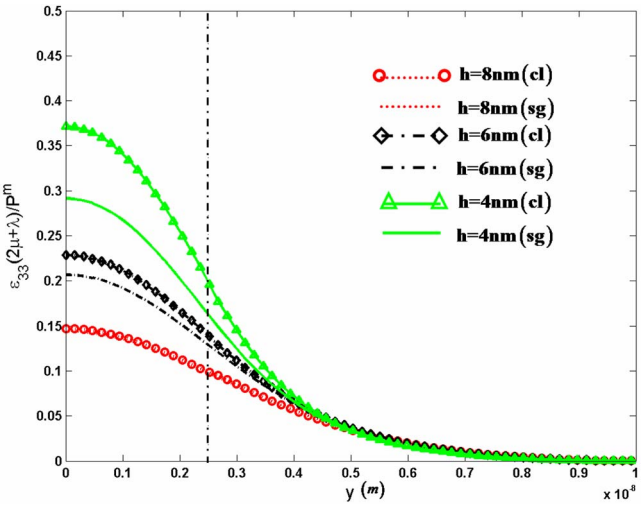

FIG. 12. (Color online) Size sensitivity to height of cylindrical QD. [h=8 nm (cl) overlaps with h=8 nm (sg).]

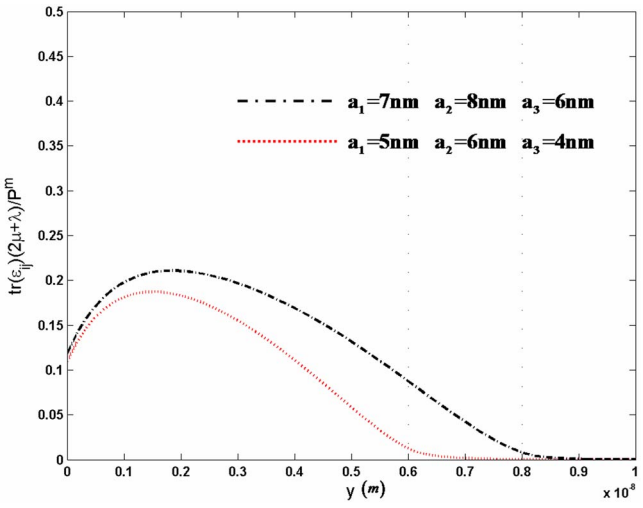

FIG. 14. (Color online) Strain dilation along y axis.

(14) has a closed-form expression. The complete solution for the strain field of an infinite cylindrical quantum dot is provided in the Appendix. In this section, a finite-length cylindrical QD is analyzed (which is common in template-grown quantum dots).

The spatial variation of the dilation is depicted in Fig. 10 for two different sized quantum dots.

The individual components of strain are provided in Fig. 11. Our solution exhibits considerable deviation from the classical result for ε_{11} and ε_{22}. However, the strain gradient result for ε_{33} is nearly the same as the classical result. Conforming to intuition, ε_{33} is sensitive to the height of the cylinder especially in the scale of a few nanometers. ε_{33} for different h are plotted in Fig. 12, which illustrates that the nonlocal results for ε_{33} begin to deviate from the classical result as the height of the QD is decreased until it is comparable to its diameter (aspect ratio of ~1). The magnitude of ε_{33} decreases with increase in height and eventually drops to zero for a QD of infinite height (i.e., a quantum wire). This is consistent with the solution of an infinite circularly cylindrical quantum wire presented in the Appendix. This result is entirely expected as for larger and larger "h," the out-of-plane strain is expected to be more homogeneous and thus impervious to strain gradient elasticity.

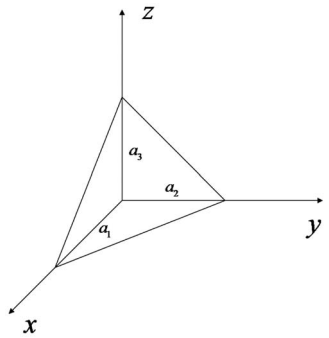

FIG. 13. Schematic figure of orthogonal polyhedral QD.

C. Polyhedral quantum dots

We conclude this section with a discussion of nonlocal effects in general polyhedral shape which is fairly common for self-assembled quantum dots. As shown in Ref. 74 all polyhedral shapes can always be subdivided into one special polyhedral shape with orthogonal axes as indicated in Fig. 13.

The dilation of strain is plotted along (010) which is also one of the edges of the QD. Figure 14 show the dilation for two different sized QDs while the individual strain components are shown in Fig. 15.

VI. ANISOTROPY: NUMERICAL RESULTS

In this section we present some illustrative results accounting for anisotropic effects. As is readily evident from our general formulation in Sec. IV, in strain gradient or nonlocal elasticity, accounting for anisotropic effects is somewhat complex. Referring to Sec. IV, the results in the present

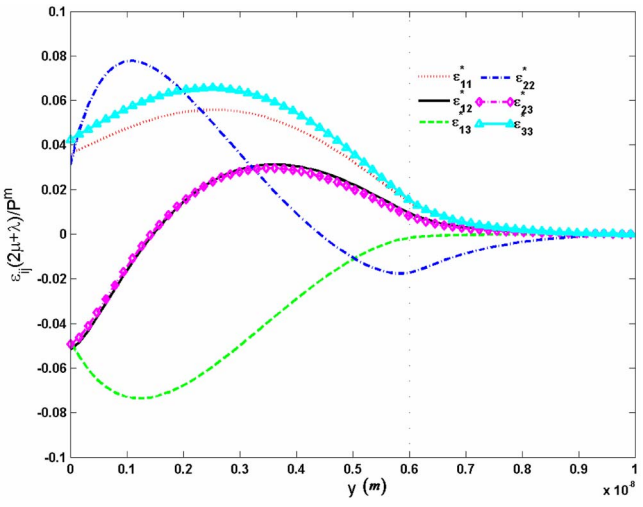

FIG. 15. (Color online) Strain components along (010) of orthogonal polyhedron with a_1=5 nm, a_2=6 nm, a_3=4 nm.

TABLE I. Elastic parameters for GaAs.

	Classical isotropic	Classical cubic anisotropic[a]	Isotropic strain gradient	Cubic strain gradient[b]
C_{1111} (N/m^2) ($\times 10^{11}$)	1.18	1.18	1.18	1.18
C_{1122} ($\times 10^{11}$)	0.245	0.56	0.245	0.56
C_{1212} ($\times 10^{11}$)	0.59	0.59	0.59	0.59
d_{12223} (N/m)	0	0	0	0
f_{111111} (N) ($\times 10^{-8}$)	0	0	7.93	7.93
f_{122122} ($\times 10^{-8}$)	0	0	3.97	3.97
f_{112222} ($\times 10^{-8}$)	0	0	0.99	0.99
f_{122133} ($\times 10^{-8}$)	0	0	0.66	0.66
f_{112233} ($\times 10^{-8}$)	0	0	0.33	0.33
f_{211222} ($\times 10^{-8}$)	0	0	1.983	1.983

[a]Parameters are taken from Ref. 63.
[b]Parameters are calculated based on isotropic average relationship in Ref. 63.

section are based on Eqs. (36)–(39). To be more explicit about our numerical results, Eq. (37) is written in matrix form as

$$\begin{bmatrix} D_{11} & D_{12} & D_{13} \\ D_{21} & D_{22} & D_{23} \\ D_{31} & D_{32} & D_{33} \end{bmatrix} \begin{bmatrix} \hat{u}_1 \\ \hat{u}_2 \\ \hat{u}_3 \end{bmatrix} = \begin{bmatrix} -iP_{11}^m q_1 \\ -iP_{22}^m q_2 \\ -iP_{33}^m q_3 \end{bmatrix} \hat{\chi}(\mathbf{q}). \tag{41}$$

Alternatively, the following form is useful for computation:

$$\begin{bmatrix} \hat{u}_1 \\ \hat{u}_2 \\ \hat{u}_3 \end{bmatrix} = \begin{bmatrix} D_{11} & D_{12} & D_{13} \\ D_{21} & D_{22} & D_{23} \\ D_{31} & D_{32} & D_{33} \end{bmatrix}^{-1} \begin{bmatrix} -iP_{11}^m q_1 \\ -iP_{22}^m q_2 \\ -iP_{33}^m q_3 \end{bmatrix} \hat{\chi}(\mathbf{q}). \tag{42}$$

DiVincenzo[63] attempted to provide detailed strain gradient parameters for GaAs through atomistic simulations but (as pointed out by himself) since atomistic potentials are rarely calibrated to include nonlocal effects, those values are highly suspect. He, however, does provide (based on experimental results) isotropic averages of the higher order tensors from which we can deduce the average length scale (see Appendix, 0.82 nm).Thus we consider classical elastic constants that are anisotropic but use an average length scale. We hasten to point out that this is not the limitation of our models but rather availability of the pertinent parameters.

To isolate the anisotropic effects, we choose shapes of high symmetry for illustrative purposes (e.g., finite-length cylinder and spherical shape). Some relevant material parameters are summarized in Table I.

We analyze two cases.

(a) Finite-length cylinder: sample QD is chosen with $D=4$ nm and $h=6$ nm. Strain components are depicted in Figs. 16(a)–16(c).

(b) Spherical QD: The sample QD is chosen with radius equal to 2 nm. Figures 16(d)–16(f) plot three components of strain ε_{11}, ε_{22}, and ε_{33} along the radius of the QD.

As can be readily seen, the isotropic formulation overestimates the strain state. Interestingly, the difference between isotropic strain gradient and anisotropic strain gradient is generally less than the difference between the isotropic classical elastic and cubic classical elastic cases.

VII. A BRIEF NOTE ON IMPLICATIONS FOR ELECTRONIC BAND STRUCTURE

A detailed study on how the modified *size-dependent* strain state due to nonlocal interactions affects the band structure is beyond the scope of the present work. A typical procedure, used for zinc-blende semiconductors in several references, is to employ the $\mathbf{k}\cdot\mathbf{p}$ framework. Most work essentially uses the Bir-Pikus[75] Hamiltonian or some modification of it. The reader is referred to Bahder[76] and Pollak[77] for a good review on this subject in addition to the book by Singh.[26] Several other works can be consulted as well that utilize this multiband $\mathbf{k}\cdot\mathbf{p}$ approach (e.g., Jiang and Singh,[78] Pryor,[79] and Zunger[80]). Rather than use such an approach for detailed electronic calculations in the present context, we shall simply provide the reader with a rough feel for the impact that inclusion of nonlocal interactions may have on band structure. Most works that discuss linking of strain to band structure calculations (including the aforementioned references) use a Hamiltonian that omits strain gradient effects. Clearly, the latter is important in the context of our work. Zhang[81] has remedied the conventional approach and has derived a general Hamiltonian that perturbatively incorporates strain gradient terms also. However, the additional gradient terms in his Hamiltonian (while obviously of crucial importance in our case) are tedious to implement and as such a more in-depth study of the use of the Zhang Hamiltonian is relegated to a future study.

Careful calculation based on a multiband envelope function requires calculation of eight coupled Schrödinger's equations.[79] Merely for illustration, we present a simple single-band calculation. There is no illusion in the authors' mind regarding the accuracy of a single-band approach; however, since a rigorous implementation in any case must await the full development of Zhang's Hamiltonian, a simple approximation is used that will serve to highlight the relative

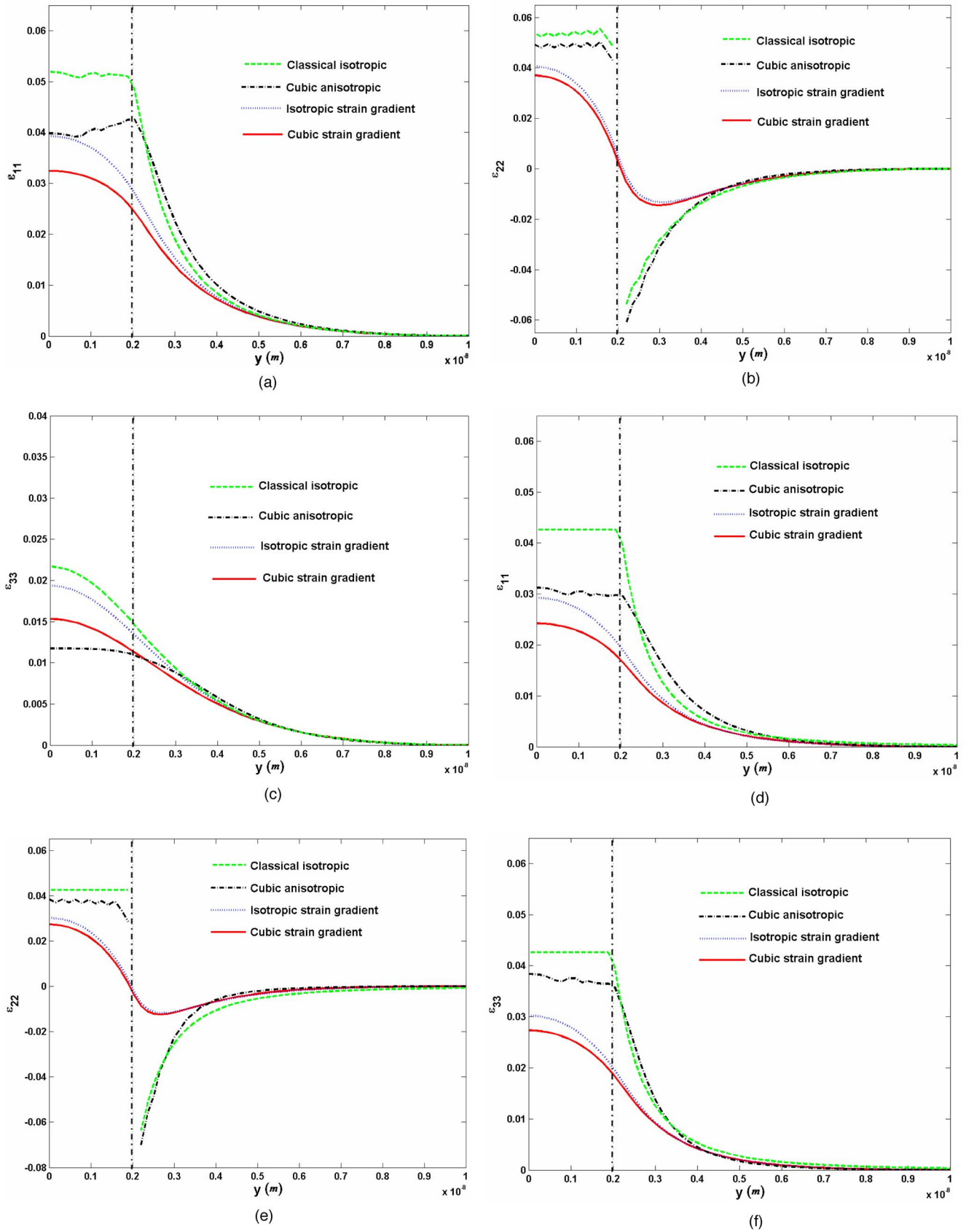

FIG. 16. (Color online) Strain component of finite cylinder QD for different cases (a) ε_{11}, (b) ε_{22}, (c) ε_{33}. Strain components of sphere QD for different cases (d) ε_{11}, (e) ε_{22}, (f) ε_{33}. (In the classical isotropic case, ε_{33} should be equal to ε_{11} due to symmetry, which is indicated here. However, it is different for the anisotropic case.)

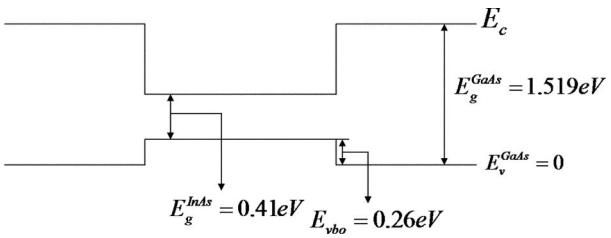

FIG. 17. Unstrained band profile for InAs/GaAs quantum dot heterogeneous system. Figures are chosen from Ref. 82, while E_v^{GaAs} is set to 0 eV.

differences in implications for electronic structure calculations depending upon whether or not nonlocal effects are incorporated.

We solve the standard effective mass equations

$$-\frac{\hbar^2}{2m_{ij}}\partial_j\partial_i\psi + V(\boldsymbol{\varepsilon})\psi = E\psi, \tag{43}$$

where m_{ij} is the effective mass for the conduction or valence band. $V(\varepsilon)$ is the potential due to the strain effect.

In this simple approximation, for a conduction band, $m_{ij} = m^* m_0 \delta_{ij}$ (m_0 is the electron mass) due to s symmetry the strain potential becomes

$$V(\boldsymbol{\varepsilon}) = a_c \mathrm{Tr}(\varepsilon_{ij}) \tag{44}$$

where a_c is conduction band deformation potential constant.

For the valence band we have

$$V(\boldsymbol{\varepsilon}) = a_v \mathrm{Tr}(\boldsymbol{\varepsilon}) - \frac{b}{2}(\varepsilon_{11} + \varepsilon_{22} - 2\varepsilon_{33}) \tag{45}$$

where a_v and b are valence band deformation potential constants. In this case the effective mass matrix is anisotropic, which has nonzero components

$$m_{xx,yy} = -m_{hh}^{xy} m_0, \quad m_{zz} = -m_{hh}^{z} m_0.$$

We assess the impact of nonlocal corrections on a buried spherical quantum dot (InAs/GaAs system). Again, the barrier size is chosen large enough to preclude any boundary effects (for ease of interpretation of results). The unstrained potential profiles due to band edge offsets between the quantum dot and the matrix are illustrated in Fig. 17.

The various parameters used the electronic calculations are listed in Table II.

The relevant equations are solved using the finite-element

TABLE II. Parameters required for calculation.

	Electron	Hole	
Effective mass	m^*	m_{hh}^{xy}	m_{hh}^{z}
GaAs	0.0665	0.112	0.0377
InAs	0.023	0.035	0.0341
Deformation potential	a_c (eV)	a_v (eV)	b (eV)
GaAs	−7.17	1.16	−1.6
InAs	−5.08	1	−1.8

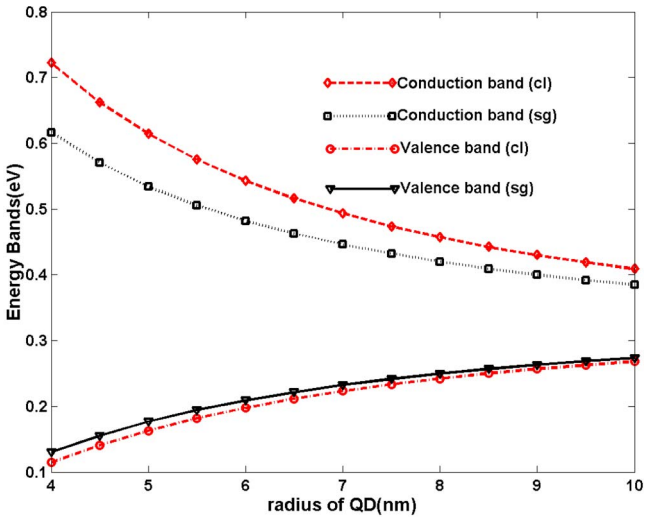

FIG. 18. (Color online) Band energy for different size QDs.

method via the commercial software FEMLAB. The conduction and valence band energies are computed for different sizes and shown in Fig. 18. We have excluded sizes below 4 nm as we are skeptical about the validity of even an eight-band model for such small sizes, let alone a single-band model.

In the spirit of a relative comparison, we note two results of interest in Fig. 18: (1) the valence band appears to be relatively unaffected by nonlocal effects and for "large" quantum dot size very quickly becomes indistinguishable from results predicated on classical elasticity; (2) the conduction band, however, shows significant shifts and thus we can accordingly expect shifts in band gaps and optical activity as well. For a size 4 nm quantum dot, a discrepancy of ~100 meV is predicted which eventually reduces to about 25 meV for about a size of 10 nm. To illustrate the square of the wave function distribution, we select a quantum dot of size 5 nm and plot it along with the relevant energy levels in Fig. 19.

It can be observed from Fig. 19 that carriers (hole or electron) are confined in the quantum dot area for the ground

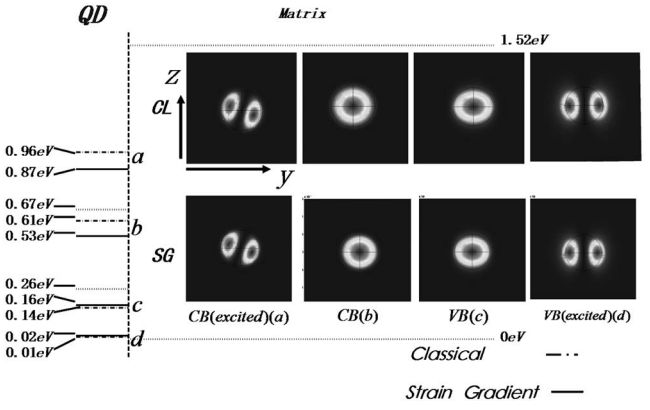

FIG. 19. Band energies and carrier density $|\psi|^2$ for QD with radius equal to 5 nm. The central areas (dark gray) indicate higher numbers for the contour plot for carrier density. These results are for a slice of the y-z plane.

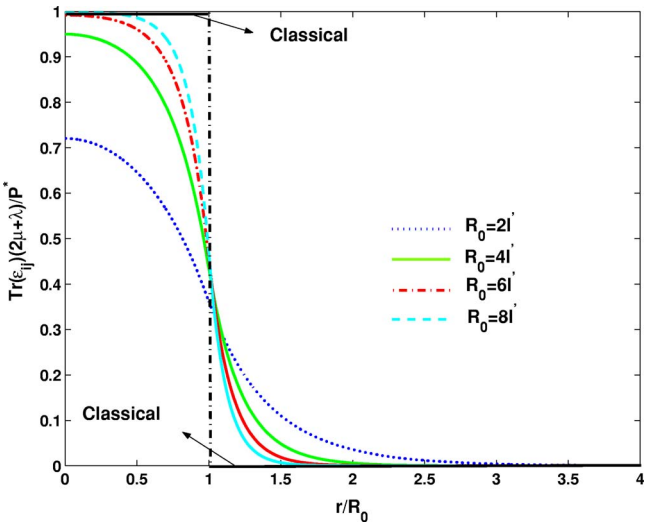

FIG. 20. (Color online) Dilation strain of a cylindrical quantum wire.

and the first excited states. Apparently, nonlocal corrections do not qualitatively change the wave function distribution and only numerical values of the eigenenergies are shifted. This conclusion, of course, is somewhat premature given the simplistic nature of the band energy model employed. A more detailed study on electronic structure calculations is relegated to a future study.

VIII. SUMMARY AND CONCLUSIONS

To summarize, we have discussed the size dependency of strain in lattice-mismatched embedded quantum dots based on the mechanism of nonlocal interactions (included in the form of higher-order strain gradients). Analytical results are presented for spherical shaped quantum dots and cylindrical quantum wires. Apart from the formal contributions, we note in particular that the size effects due to nonlocal interactions can be rather appreciable for sub-10-nm sized structures. In particular we presented results for GaAs for which an estimate of the strain gradient parameter is available. Nevertheless, we emphasize here that the severity of the impact of nonlocal results crucially depends upon the length scale parameter and the latter must be accurately found for the material of interest.

Further, in the present work, various shapes were considered. Some illustrative results are shown for shapes such as a finite cylindrical quantum dot, pyramidal, cuboidal, etc. In particular, a rather simple result is obtained for the dilation. Material anisotropy is also duly incorporated in our formulation. We finally note that while detailed electronic band structure calculations were not carried out, it is estimated that errors in the hundreds of meV can be incurred in the sub-10-nm size range if nonlocal effects are ignored. Qualitatively, our nonlocal solutions exhibit strain profiles that are more physical than those obtained from classical elasticity (i.e., discontinuities across interfaces are smoothed out and singularities in the cases of corners in polyhedral shapes are eliminated).

ACKNOWLEDGMENT

We acknowledge support of the ONR Award No. N000140510662.

APPENDIX: DISCUSSION OF STRAIN GRADIENT SOLUTION OF INFINITE CYLINDRICAL SHAPE INCLUSION (NANOWIRE) IN AN ISOTROPIC MEDIUM

Apart from the spherical shape, an infinitely long circularly cylindrical quantum wire is the other shape for which closed-form analytical results are available. Yukawa potential for this shape has already been evaluated by Cheng and He[55] in a different context:

$$M(\mathbf{x},k)=\begin{cases} krI_1\left(\frac{r}{k}\right)K_0\left(\frac{r}{k}\right)+krI_0\left(\frac{r}{k}\right)K_1\left(\frac{r}{k}\right)-kR_0K_1\left(\frac{R_0}{k}\right)I_0\left(\frac{r}{k}\right), & r\in\Omega, \\ kR_0I_1\left(\frac{R_0}{k}\right)K_0\left(\frac{r}{k}\right), & r\notin\Omega. \end{cases} \tag{A1}$$

The displacement field of this quantum wire is then

$$u_i=-\frac{1}{\mu}(\phi_{,k}-M_{,k})P^m_{ik}+\frac{P^m_{jk}}{\mu}\partial_i\partial_j\left(\frac{\psi_{,ijk}}{2}+l^2\phi_{,ijk}-l^2M_{,ijk}\right)-\frac{P^m_{jk}}{2\mu+\lambda}\left(\frac{\psi_{,ijk}}{2}+l'^2\phi_{,ijk}-l'^2M_{,ijk}\right). \tag{A2}$$

For hydrostatic lattice mismatch strain, this is simplified to

$$u_i=P^m\left[-\frac{1}{\mu}(\phi_{,i}-M_{,i})+\frac{1}{\mu}\nabla^2\left(\frac{\psi_{,i}}{2}+l^2\phi_{,i}-l^2M_{,i}\right)-\frac{1}{2\mu+\lambda}\nabla^2\left(\frac{\psi_{,i}}{2}+l'^2\phi_{,i}-l'^2M'_{,i}\right)\right]. \tag{A3}$$

Further simplification yields

$$u_i = -\frac{1}{2\mu+\lambda}(\phi_{,i} - M'_{,i})P^m. \tag{A4}$$

The strain is

$$\varepsilon_{ij} = -\frac{1}{2\mu+\lambda}(\phi_{,ij} - M'_{,ij})P^m. \tag{A5}$$

Finally the dilatation of the quantum wire is given as

$$Tr(\varepsilon_{ij}) = \begin{cases} \dfrac{P^m}{(2\mu+\lambda)}\left[\dfrac{r}{l'}I_1\left(\dfrac{r}{l'}\right)K_0\left(\dfrac{r}{l'}\right) + \dfrac{r}{l'}I_0\left(\dfrac{r}{l'}\right)K_1\left(\dfrac{r}{l'}\right) - \dfrac{R_0}{l'}K_1\left(\dfrac{R_0}{l'}\right)I_0\left(\dfrac{r}{l'}\right)\right], & r \in \Omega, \\ \dfrac{P^m}{(2\mu+\lambda)}\left[\dfrac{R_0}{l'}I_1\left(\dfrac{R_0}{l'}\right)K_0\left(\dfrac{r}{l'}\right)\right], & r \notin \Omega, \end{cases} \tag{A6}$$

where R_0 is the radius of the quantum wire (see Fig. 20).

*Email address: psharma@uh.edu

[1] S. Nakamura, S. Pearton, and G. Fasol, *The Blue Laser Diode: The Complete Story* (Springer, Berlin, 2002).
[2] Y. Arakawa, IEEE J. Sel. Top. Quantum Electron. **8**, 823 (2002).
[3] D. G. Deppe and D. L. Huffaker, Appl. Phys. Lett. **77**, 33252000).
[4] P. Bhattacharya, Opt. Quantum Electron. **32**, 211 (2000).
[5] Y. Chye, M. E. White, E. Johnston-Halperin, B. D. Gerardot, D. D. Awschalom, and P. M. Petroff, Phys. Rev. B **66**, 201301(R) (2002).
[6] T. Lundstrom, W. Sheonfeld, H. Lee, and P. M. Petroff, Science **286**, 2312 (1999).
[7] P. M. Petroff, Top. Appl. Phys. **90**, 1 (2003).
[8] P. Alivisatos, *Semiconductor Nanocrystals: From Scaling Laws to Biological Applications*, Conference on Quantum Electronics and Laser Science (QELS) (Technical Digest Series, 2000).
[9] P. Bhattacharya, A. D. Stiff-Roberts, S. Krishna, and S. Kennerly, Int. J. High Speed Electron. Syst. **12**, 969 (2002).
[10] D. Bimberg, M. Grandmann, and N. N. Lendenstov, *Quantum Dot Heterostructures* (Wiley, New York, 1996).
[11] D. Bimberg, Semiconductors **33**, 951 (1999).
[12] J. Tersoff, C. Teichert, and M. G. Lagally, Phys. Rev. Lett. **76**, 1675 (1996).
[13] A. J. Williamson and A. Zunger, Phys. Rev. B **58**, 6724 (1998).
[14] M. Grundmann, O. Stier, and D. Bimberg, Phys. Rev. B **52**, 11969 (1995).
[15] S. Bandhyopadhyay and H. S. Nalwa, *Quantum Dots and Nanowires* (American Scientific Publishers, CA, 2003).
[16] F. Glas, J. Appl. Phys. **90**, 3232 (2001).
[17] H. T. Johnson and L. B. Freund, Int. J. Solids Struct. **38**, 1045 (2001).
[18] J. R. Downes, D. A. Faux, and E. P. O'Reilly, J. Appl. Phys. **81**, 6700 (1997).
[19] J. H. Davies, J. Appl. Phys. **84**, 1358 (1998).
[20] L. B. Freund and H. T. Johnson, J. Mech. Phys. Solids **49**, 1925 (2001).
[21] P. Sharma and S. Ganti, Phys. Status Solidi B **233**, R10 (2002).
[22] A. E. Romanov, G. E. Beltz, W. T. Fischer, P. M. Petroff, and J. S. Speck, J. Appl. Phys. **89**, 4523 (2001).
[23] E. Pan and B. Yang, J. Appl. Phys. **90**, 6190 (2001).
[24] M. Yang, J. C. Sturm, and J. Prevost, Phys. Rev. B **56**, 1973 (1997).
[25] S. W. Ellaway and D. A. Faux, J. Appl. Phys. **92**, 3027 (2002).
[26] J. Singh, *Physics of Semiconductors and Their Heterostructures* (McGraw-Hill Higher Education, New York, 1992).
[27] J. K. Diao, K. Call, and M. L. Dunn, J. Mech. Phys. Solids **52**, 1935 (2004).
[28] P. Sharma and S. Ganti, J. Appl. Mech. **71**, 663 (2004).
[29] P. Sharma, S. Ganti, and N. Bhate, Appl. Phys. Lett. **82**, 535 (2003).
[30] R. Dingreville, J. M. Qu, and M. Cherkaoui, J. Mech. Phys. Solids **53**, 1827 (2005).
[31] S. Cuenot, C. Fretigny, S. Demoustier-Champagne, and B. Nysten, Phys. Rev. B **69**, 165410 (2004).
[32] L. H. He, C. W. Lin, and B. S. Wu, Int. J. Solids Struct. **41**, 847 (2004).
[33] C. W. Lin and L. H. He, Int. J. Mech. Sci. **46**, 1715 (2004).
[34] R. C. Cammarata and K. Sieradzki, Annu. Rev. Mater. Sci. **24**, 215 (1994).
[35] C. Morant, S. Garcia-Manyes, F. Sanz, J. M. Sanz, and E. Elizalde, Nanotechnology **16**, S211 (2005).
[36] T. C. Chang and H. J. Gao, J. Mech. Phys. Solids **51**, 1059 (2003).
[37] H. L. Duan, J. Wang, Z. P. Huang, and B. L. Karihaloo, J. Mech. Phys. Solids **53**, 1574 (2005).
[38] D. C. C. Lam, F. Yang, A. C. M. Chong, J. Wang, and P. Tong, J. Mech. Phys. Solids **51**, 1477 (2003).
[39] C. T. Sun and H. T. Zhang, J. Appl. Phys. **93**, 1212 (2003).
[40] R. E. Miller and V. B. Shenoy, Nanotechnology **11**, 139 (2000).
[41] A. Alizadeh, P. Sharma, S. Ganti, S. LeBoeuf, and L. Tsakalakos, J. Appl. Phys. **95**, 8199 (2004).
[42] Note that the mismatch strain ε^m must be subtracted from Eq. (1) before employing it in band structure calculations; however, in the present work we will simply present the total elastic strain. Those using the present results for electronic calculations or comparing to other works, e.g., Ref. 24, should keep this fact in mind.
[43] H. Ibach, Surf. Sci. Rep. **29**, 193 (1997).

[44] M. E. Gurtin and A. I. Murdoch, Arch. Ration. Mech. Anal. **57**, 291 (1975).
[45] M. E. Gurtin, J. Weissmuller, and F. Larche, Philos. Mag. A **78**, 1093 (1998).
[46] P. Muller and A. Saul, Surf. Sci. Rep. **54**, 157 (2004).
[47] C. Eringen, *Non-Local Continuum Field Theories* (Springer-Verlag, New York, 2002).
[48] H. Kleinert, *Gauge Fields in Condensed Matter*, 2nd ed. (World Scientific, Singapore, 1989).
[49] Indeed, the gradients of ω are admissible since those fields are invariant with respect to the Euclidean group of transformations SO(3) and T(3) unlike ω itself.
[50] R. D. Mindlin, Int. J. Solids Struct. **1**, 417 (1965).
[51] T. Mura, *Micromechanics of Defects in Solids* (Martinus Nijhoff, Hague, The Netherlands, 1987).
[52] O. D. Kellogg, *Foundation of Potential Theory* (Dover, New York, 1953).
[53] G. W. Gibbsons and B. F. Whiting, Nature (London) **291**, 636 (1981).
[54] Z. Q. Cheng and L. H. He, Int. J. Eng. Sci. **33**, 389 (1995).
[55] Z. Q. Cheng and L. H. He, Int. J. Eng. Sci. **35**, 659 (1997).
[56] J. D. Eshelby, Proc. R. Soc. London, Ser. A **241**, 376 (1957).
[57] D. A. Faux, J. R. Downes, and E. P. O'Reilly, J. Appl. Phys. **82**, 3754 (1997).
[58] A. D. Prins and D. J. Dunstan, Philos. Mag. Lett. **58**, 37 (1988).
[59] R. W. Keyes, J. Appl. Phys. **33**, 3371 (1962).
[60] A. D. Andreev, J. R. Downes, and D. A. Faux, J. Appl. Phys. **86**, 297 (1999).
[61] A. C. Eringen, *Nonlocal Continuum Field Theories* (Springer, New York, 2002).
[62] B. Altan and E. C. Aifantis, Scr. Metall. Mater. **26**, 319 (1992).
[63] D. P. DiVincenzo, Phys. Rev. B **34**, 5450 (1986).
[64] Here we simply adopt scalar notation to merely emphasize the concept.
[65] A. Lenz, R. Timm, H. Eisele, C. H. Hennig, S. K. Becker, R. L. Sellin, U. W. Pohl, D. Bimberg, and M. Dahne, Appl. Phys. Lett. **81**, 5150 (2002).
[66] M. Moreno, A. Trampert, B. Jenichen, L. Daweritz, and K. H. Ploog, J. Appl. Phys. **92**, 4672 (2002).
[67] M. S. Miller, J-O. Malm, M. E. Pistol, S. Jeppesen, B. Kowalski, K. Georgsson, and L. Samuelson, J. Appl. Phys. **80**, 3360 (1996).
[68] Q. Xie, A. Madhukar, P. Chen, and N. P. Kobayashi, Phys. Rev. Lett. **75**, 2542 (1995).
[69] G. S. Solomon, J. A. Trezza, A. F. Marshall, and J. S. Harris, Jr., Phys. Rev. Lett. **76**, 952 (1996).
[70] L. N. Trefethen, *Spectral Methods in Matlab* (SIAM, Philadelphia, 2000).
[71] Y. P. Chiu, J. Appl. Mech. **44**, 587 (1977).
[72] G. Faivre, Phys. Status Solidi **35**, 249 (1964).
[73] D. Gottlieb and C. W. Shu, SIAM Rev. **39**, 644 (1997).
[74] H. Nozaki and M. Taya, J. Appl. Mech. **68**, 441 (2001).
[75] G. L. Bir and G. E. Pickus, *Symmetry and Strain Induced Effects in Semiconductors* (John Wiley, New York, 1974).
[76] T. B. Bahder, Phys. Rev. B **45**, 1629 (1992).
[77] F. H. Pollak, in *Strained-Layer Superlattices*, edited by T. Pearsall, Semiconductors and Semimetals (Academic, Boston, 1990).
[78] H. Jiang and J. Singh, Phys. Rev. B **56**, 4696 (1997).
[79] C. Pryor, Phys. Rev. B **57**, 7190 (1998).
[80] A. Zunger, MRS Bull. **23**, 35 (1998).
[81] M. Yu, Y. Kakehashi, and H. Tanaka, Phys. Rev. B **49**, 352 (1994).
[82] M. Grundmann, O. Stier, and D. Bimberg, Phys. Rev. B **52**, 11969 (1995).